Superconducting fluctuations and the Nernst effect in high-T_c superconductors

2013 Supercond. Sci. Technol. 26 105029

(http://iopscience.iop.org/0953-2048/26/10/105029)

Supercond. Sci. Technol. **26** (2013) 105029 (7pp) doi:10.1088/0953-2048/26/10/105029

Superconducting fluctuations and the Nernst effect in high-T_c superconductors

Y-J Chen[1], P J Lin[2], K H Wu[1], B Rosenstein[1], C W Luo[1], J Y Juang[1] and J-Y Lin[3]

[1] Department of Electrophysics, National Chiao Tung University, Hsinchu 300, Taiwan
[2] Research Department, Universal Analytics Inc., Airdrie, AB, Canada
[3] Institute of Physics, National Chiao Tung University, Hsinchu 300, Taiwan

E-mail: khwu@cc.nctu.edu.tw, cwluo@mail.edu.tw and ago@cc.nctu.edu.tw (J-Y Lin)

Received 6 June 2013, in final form 7 August 2013
Published 12 September 2013
Online at stacks.iop.org/SUST/26/105029

Abstract
The comprehensive $\rho(T)$ measurements and the consequent resistivity curvature mapping (RCM) on $Y_{0.7}Ca_{0.3}Ba_2Cu_3O_{7-\delta}$ thin films (doping levels $p = 0.08$–0.21) elucidate a phase diagram for the whole doping range. This phase diagram further strengthens a view that the 'normal' phase in hole-doped cuprates should be divided into a strong superconducting (SC) fluctuation phase and the 'real' normal phase in which there is no significant influence of SC. The temperature of superconducting fluctuations T_f as a function of p was calculated using the Ginzburg–Landau model for layered superconductors. Comparisons between T_f and the Nernst temperature establish the origin of the Nernst effect as SC fluctuations. Some of the details in $\rho(T)$ cannot be fully understood by the existing models and call for a more sophisticated theory of carrier dynamics in cuprates.

(Some figures may appear in colour only in the online journal)

1. Introduction

The investigation of high-T_c superconductors has provided a long list of unexpected results on the path to elucidate the mechanism of superconductivity. However, various physical phenomena complicate this task: the unconventional d-wave superconducting gap symmetry, quasi-2D nature of the Fermi surface, pseudogap (PG) and the large thermal fluctuations among others.

Recently an unexpectedly large Nernst signal (voltage induced by the temperature gradient under magnetic fields) well above T_c was observed in both low-T_c (but strongly fluctuating) [1, 2] and high-T_c [3, 4] superconductors. The Nernst effect is caused by the combination of at least three factors: (1) the motion of vortices in the vortex-liquid regime, (2) superconducting fluctuations in the normal state and (3) a quasiparticle contribution. The disentanglement of (2) and (3) was just achieved not long ago (see, e.g. [4]). More recently the AC conductivity and diamagnetic signal have further strengthened a view that the normal phase in these materials should be divided qualitatively into a strong superconducting (SC) fluctuations phase (extending up to a certain crossover temperature $T_f > T_c$) and the 'real' normal phase in which there is no significant influence of SC [5–8]. T_f most probably is not related to other normal state crossover temperatures like the PG temperature (T^*). The determination of T_f as function of doping concentration p in various compounds is therefore an important physical question. One wonders whether more conventional transport experiments like the DC conductivity measurement are as sensitive to $T_f(p)$ as they are to $T^*(p)$. Recently, the onset temperatures T_f for three different doping levels in YBCO single crystals were identified by microwave absorption experiments with applied magnetic fields [5]. These results demonstrated the opposite tendency of $T_f(p)$ compared to that of $T^*(p)$, especially in the deeply underdoped region (for example $T_f = 80$ K $\ll T^* \sim$ 270 K at $p = 0.10$). The high field resistivity studies in both YBCO [9] and LSCO [10] have also suggested the opposite trends of $T_f(p)$ and $T^*(p)$.

Unfortunately, the doping dependence of $T^*(p)$ of hole-doped cuprates has not been determined until now. The PG line determined by a variety of techniques has been generally classified into three types. In the first type, the PG line $T^*(p)$ intersects the superconducting dome at about optimum doping p_o [11]; in the second type, $T^*(p)$ merges gradually with the superconducting transition line

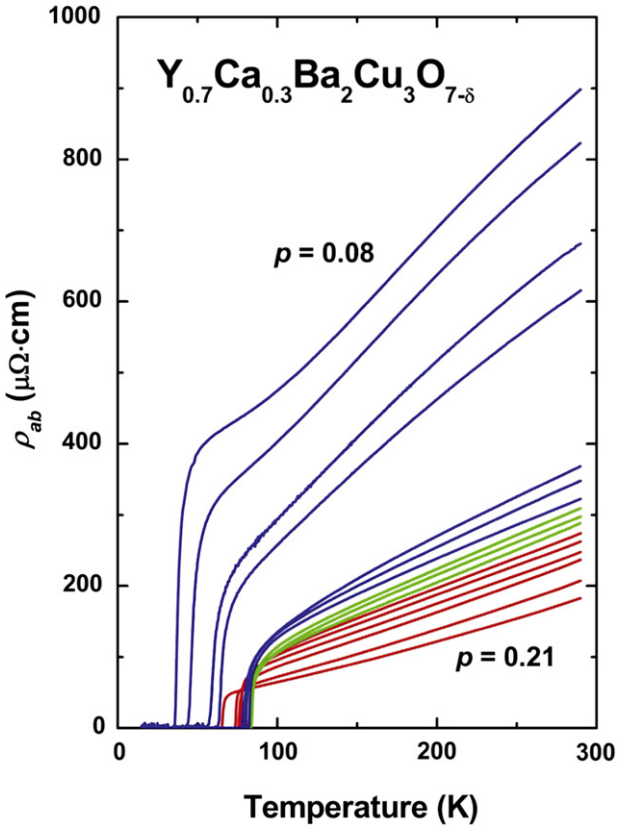

Figure 1. Temperature dependence of the in-plane resistivity $\rho_{ab}(T)$ for $Y_{0.7}Ca_{0.3}Ba_2Cu_3O_{7-\delta}$ thin films with various hole concentration $p = 0.08$–0.21; downward (blue), T-linear (green) and upward (red) curves at high temperature stand for underdoped, optimally doped, and overdoped samples, respectively.

$T_c(p)$ in the heavily overdoped regime [12]; most recently, for the third type, investigations in Nd-LSCO, Eu-LSCO and YBCO, [13–15] presented the $T^*(p)$ somewhat between the former two types. Therefore, the study of resistivity as a function of temperature in the overdoped regime may shed light on this issue as well as on the SC fluctuations.

In this paper, the temperature dependence of electric resistivity of a series of Ca-doped YBCO ($Y_{0.7}Ca_{0.3}Ba_2Cu_3O_{7-\delta}$) films has been measured over a wide range of doping concentrations as shown in figure 1. $T_f(p)$ was determined using the phenomenological Ginzburg–Landau (GL) fluctuation theory from conductivity data. The use of the GL renormalized theory, instead of other models that depend on the (still uncertain) microscopic mechanism, makes it possible to capture the universal properties of thermal fluctuations parameterized mostly by the Ginzburg number Gi [16]. Finally, a comprehensive survey of the resistivity curvature mapping (RCM) [17] was conducted for tracking the PG line and other previously unresolved issues.

2. Sample preparation and characterization

In general, there are two methods to alter the hole concentration on the CuO_2 planes of YBCO. One is to take away the oxygen from Cu–O chains in YBCO. The other provides extra holes by replacing Y^{3+} with Ca^{2+}, which increases the hole concentration. In this study, the Ca was doped into YBCO to provide a wider tunable range of the hole concentration. A nominal Ca-doped YBCO target was prepared following the solid-state reaction from high-purity (4N) Y_2O_3, CuO, $BaCO_3$ and $CaCO_3$ powder. The Ca-doped YBCO thin films were prepared on (100) $SrTiO_3$ substrates using pulsed laser deposition (PLD) at 760 °C with the oxygen pressure of 0.3 Torr. The pulse energy density and repetition rate of KrF excimer laser ($\lambda = 248$ nm) are approximately 3 J cm^{-2} and 5 Hz, respectively. The thickness of (001)-oriented Ca-doped YBCO thin films on $SrTiO_3$(100) substrates is approximately 3000 Å. After deposition, the film was cooled in the chamber full of oxygen to room temperature with the heater off. The crystallinity of the film was analyzed by measuring the x-ray diffraction (XRD) pattern. In order to ascertain the resistivity, the thin film was further etched to a micro-bridge via photolithography. The temperature-dependent resistivity $\rho(T)$ of Ca-doped YBCO films with various hole concentration p were systematically measured by a standard four-probe method as shown in figure 1. The hole concentration of these films was estimated using the empirical formula $\frac{T_c}{T_{c,max}} = 1 - 82.6(p-0.16)^2$ [18], where $T_{c,max} = 84$ K is the critical temperature of Ca-doped YBCO at optimal doping. The oxygen content of a single film can be repeatedly changed by controlling temperatures and oxygen pressures inside the quartz tube surrounded by the furnace [19]. After the annealing process, the quartz tube was immediately quenched to room temperature to avoid the long-range oxygen ordering phenomenon [20]. According to the method as mentioned above, all the measurements with various oxygen deficiencies from the overdoping to underdoping regimes can be achieved on just a few Ca-doped YBCO thin films. For this reason, any changes in the superconducting properties will arise mainly from the effects of the oxygen contents. Possible complications originating from individual film structures are minimized.

3. Methods of analysis

3.1. The Ginzburg–Landau theory of thermal fluctuations

Here, we use the self-consistent Ginzburg–Landau (GL) fluctuation theory recently developed to discuss the conductivity [21]. The SC order parameter Ψ contribution to conductivity is given by the Kubo formula

$$\sigma = \frac{1}{T}\int_0^\infty \langle J(0)J(t)\rangle \, \mathrm{d}t \tag{1}$$

calculated within the Gaussian approximation. The supercurrent is

$$J = \frac{ie^*\hbar}{2m^*}\left(\Psi^*\nabla\Psi - \Psi\nabla\Psi^*\right). \tag{2}$$

An equation of motion for Ψ can be obtained from the time-dependent Ginzburg–Landau equation [16, 21, 22], which describes the relaxation process of the condensate:

$$\Gamma\frac{\partial\Psi}{\partial t} = -\frac{\delta F[\Psi]}{\delta\Psi^*}. \tag{3}$$

Here Γ is the temperature-dependent relaxation time, and F is the GL free energy of the system.

The orthorhombic Ca-doped YBCO is anisotropic in the crystallographic *ab* and *c* directions, and its superconducting CuO_2 layer is situated between insulating layers. In the superconducting state, Josephson coupling is the dominant mechanism for the maintenance of a global coherent condensate among the superconducting layers. According to the XRD measurement, the films are well aligned and the crystallographic *c*-axis is perpendicular to the surface. Therefore, the anisotropy of Ca-doped YBCO crystal is well preserved. As was mentioned in the previous section, the benefit of Ca-doped YBCO is that one can alter the hole concentration in CuO_2 planes without modifying significantly the lattice structure of the Ca-doped YBCO system.

The Lawrence and Doniach (LD) model takes into account both the Josephson coupling between superconducting layers and the effect of anisotropy, which provide a good approximation and are useful in the study of Ca-doped cuprates. The LD free energy is written as

$$F = L_z \sum_{\ell=0}^{N-1} \int_S \mathrm{d}^2 r \left\{ \frac{\hbar^2}{2m_{ab}} |\nabla \Psi_\ell|^2 + \frac{\hbar^2}{2m_c s^2} |\Psi_\ell - \Psi_{\ell+1}|^2 + \alpha T_\mathrm{c} \epsilon |\Psi_\ell|^2 + \frac{\beta}{2} |\Psi_\ell|^4 \right\}. \tag{4}$$

Each effective superconducting layer normal to the z axis is indexed by ℓ. The effective coupling is controlled by s, the distance between two successive superconducting layers, the anisotropy of the sample is parameterized by $\gamma \equiv \sqrt{m_c/m_{ab}}$, and L_z is the thickness of each superconducting layer. The α and β are material parameters which can be obtained from microscopic theory and $\epsilon = T/T_\mathrm{c} - 1$. The current in our case of a thin film is uniform. Expanding the order parameter in a Fourier mode, $\Psi_\ell(x, y) = \sum_k \psi_k \mathrm{e}^{\mathrm{i}k_x x + \mathrm{i}k_y y + \mathrm{i}k_\ell \ell}$, where $k_\ell = 2\pi \ell s/L$. Here, the thickness of the sample, L, is considered large compared with both s and the coherence length. The correlation function can be written as

$$\langle J_y(0) J_y(t) \rangle = \left(\frac{e^* \hbar}{m^*} \right)^2 \sum_{k,k'} k_y k'_y \left\langle |\psi_k(0)|^2 |\psi_{k'}(t)|^2 \right\rangle. \tag{5}$$

Since ψ_k are statistically independent at different k', only terms with $k' = k$ contribute.

The effect of thermal fluctuations can be calculated from the corresponding free energy $f = -k_\mathrm{B} T \log Z$, where the partition function $Z = \int \mathcal{D}\Psi \exp(-F[\Psi]/k_\mathrm{B} T)$. The functional integral of the partition function, Z, is calculated by Gaussian approximation [21–24]. If the effect of the thermal fluctuations were small, one could take them into account perturbatively, as Aslamazov–Larkin did in the framework of the BCS theory. The perturbative calculation has been done for the Lawrence–Doniach model and the results were given in [16] and applied to magnetization in [25] (the fit however was criticized in [26]). In high-T_c superconductors one is limited to the GL approach. In regions where the lowest Landau level approximation is valid, one generally performs the self-consistent calculations (see for example the recent magnetization fit [8]). At temperatures in our experiments that are higher than T_c the perturbation theory does not work as was explained in [27]. Therefore one has to use a more complicated nonperturbative self-consistent calculation as sketched below.

The propagator is

$$P_k(\varepsilon) = \left\langle |\Psi_k|^2 \right\rangle \propto \frac{1}{k^2 + \varepsilon \xi_{ab}^2} \tag{6}$$

where $\xi_{ab}^2 = \hbar^2/2m_{ab}^* \alpha T_\mathrm{c}$ is the coherence length in the *ab*-plane at $T = 0$, and ε is the variational parameter. As we will discuss shortly, ε renormalizes ϵ in the GL free energy equation (4). By minimizing the free-energy with f respect to ε we obtain a self-consistent gap equation and the first-order expansion on interaction is

$$\varepsilon = \epsilon + 4 \sum_k P_k(\varepsilon). \tag{7}$$

Note that the summation diverges at large k and renormalization is required. We introduce a cut-off in momentum space to regularize this divergence (see details in [22]) and then renormalize the quadratic term in equation (4). In terms of the renormalized T_c rather than the 'mean field' one, T_f is related by

$$T_\mathrm{f} = \frac{T_\mathrm{c}}{1 - \Delta t}; \qquad \Delta t = 4 \sum_k P_k(0) = 4\sqrt{2Gi} \ln\left(\pi r + \sqrt{\pi^2 r^2 + 1} \right). \tag{8}$$

The dimensionless Ginzburg number characterizing the fluctuations strength is defined by [16, 21, 22] $Gi = 16\pi^3 \kappa^4 T_\mathrm{c}^2 / \Phi_0^3 H_{\mathrm{c}2}$ and $r = s/\xi_\mathrm{c}$, where $\kappa = \lambda/\xi$, and λ is the penetration depth. The renormalized gap equation takes the form

$$\varepsilon = \frac{T}{T_\mathrm{c}} - 1 + 4\sqrt{2Gi} \frac{T}{T_\mathrm{c}} \ln\left(\frac{2}{\sqrt{\varepsilon r^2} + \sqrt{\varepsilon r^2 + 4}} \right). \tag{9}$$

Returning to the time-dependent correlator in equation (5), this can be obtained from equation (3) by means of the Wiener–Khintchine theorem:

$$\left\langle \psi_k^*(0) \psi_k(t) \right\rangle = \left\langle |\psi_k|^2 \right\rangle \mathrm{e}^{-t/\tau_k}, \tag{10}$$

where

$$\tau_k = \frac{2m_{ab}^* \Gamma}{\hbar^2} \frac{1}{k^2 + \varepsilon \xi^{-2}}. \tag{11}$$

Solving equation (9) and substituting into equation (10), we make use of the Kubo formula equation (1) to find the conductivity of the superconducting component

$$\sigma_\mathrm{s} = \frac{\mathrm{e}^2}{16\hbar L_z} \frac{T/T_\mathrm{c}}{\sqrt{\varepsilon \left(\varepsilon^2 r^2 + 4 \right)}}. \tag{12}$$

This expression is used to fit the conductivity. This should be complemented by the normal electrons contribution.

3.2. Experimental determination of the fluctuation conductance above T_c

In 2003, Hussey *et al* [28–30] proposed a phenomenological scattering model based on the results of angle-dependent magneto-resistance to qualitatively understand the transport properties in $Tl_2Ba_2Cu_3O_{6+\delta}$. The resistivity can be divided into two components. One is the isotropic term with T^2 behavior related to the electron–electron scattering, while the other is the anisotropic linear term in T. The behavior of the resistivity as a function of temperature can be controlled by the competition between these two kinds of components. For example, the effect of isotropic term is greater than that of the anisotropic term while the doping level extends to the overdoped regime, and $\rho(T)$ presents the upward curvature in the normal state.

In order to figure out the normal state $\rho(T)$ in the presence of superconducting fluctuations, as a first step, we adopted an earlier approach of Ando *et al* [17] for the boundary of superconducting fluctuations. This appears in the blue region below the lower yellow short-dashed line as shown in figure 2. Then a fitting range in T between the two yellow lines ($\Delta T = 50$ K) was chosen to determine the normal state contribution. Following the model of Hussey *et al* [28–30], we used a phenomenological quadratic resistivity fit:

$$\rho_e = \rho_0 + a_1 T + a_2 T^2. \tag{13}$$

The usual Fermi liquid theory accounts the electron–electron scattering which gives the $\rho \propto T^2$ dependence; the additional T-linear dependence results from the non-Fermi liquid scenario that accounts for the effect of anisotropic Fermi surface. Combined with equation (12), the total conductivity is then

$$\sigma = \sigma_s + 1/\rho_e. \tag{14}$$

The total conductivity as a function of temperature was explored within the temperature range of $T/T_c = 1.05 \sim 1.4$–2.1 (i.e., from $T/T_c = 1.05$ to the lower yellow short-dashed line as shown in figure 2). At temperatures closer to T_c the abrupt increase in conductivity hinders our analyses. The fitting results are discussed next.

4. Results and discussion

4.1. SC fluctuations and the Nernst effect

In figure 1, the blue curves represent underdoped samples ($p = 0.08$, 0.085, 0.10, 0.105 and 0.145), the green curves are optimally doped ($p = 0.15$, 0.16 and 0.17), and the red curves are overdoped ($p = 0.175$, 0.185, 0.19, 0.195, 0.20 and 0.21) samples. The doping level of a sample was determined from its critical temperature [31] and covers a wide range from underdoped to overdoped, which is well beyond the previous studies of YBCO [17]. Above the critical temperature, the resistivity of the optimally doped samples shows a linear asymptotic behavior, the underdoped samples display an upward curvature, and the overdoped samples exhibit a downward curvature.

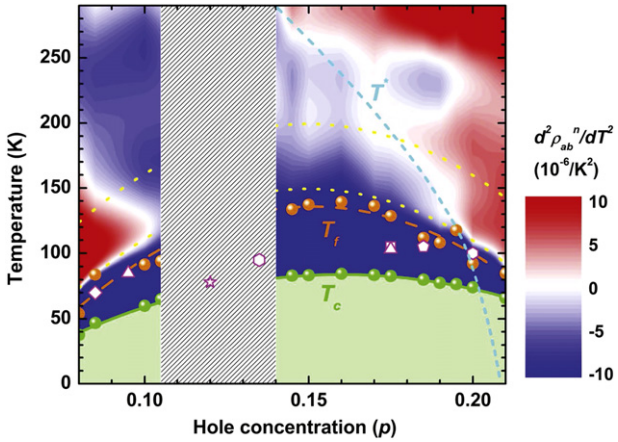

Figure 2. Phase diagram of $\rho_{ab}(T)$ for $Y_{0.7}Ca_{0.3}Ba_2Cu_3O_{7-\delta}$: curvatures of in-plane resistivity, $d^2\rho_{ab}^n/dT^2$, as a function of T and p. The resistivity of all 14 samples is normalized to 1 at $T = 290$ K. The pseudogap temperature $T^*(p)$ depicted by a light-blue dashed line is a guide to the eyes, indicating a quantum critical point at $p_c \sim 0.21$ (see text). Green open symbols denote the T_c of our measured samples. The dome-shaped area below the green line is the superconducting region. Two yellow short-dashed lines show the fitting range for the normal state contribution in resistivity. The orange points T_f denote the upper temperature of fluctuation region estimated from the superconducting fluctuation theory, where the orange dashed line is a guide to the eyes. The gray rectangular area is the hopping region under the influence of the stripe phase effect. The open symbols stand for the Nernst temperatures measured on YBCO (square [36], triangles [37], diamond [38], pentagon [39] and star [40]) and Ca-doped YBCO (hexagon [41]).

In this section, we analyze the effects of thermal fluctuations in Ca-doped YBCO. Figure 3 shows the summary of the SC fluctuation fitting on conductivity at different doping levels, e.g. $p = 0.10$ (underdoped), 0.16 (optimally doped) and 0.20 (overdoped). In order to investigate the influence of SC fluctuations in the normal state, two fitting parameters were obtained from the fitting. The first is the *Gi* number and the second is the anisotropy parameter r defined in section 3.1. The *Gi* number describing the strength of fluctuations varies from 1.2×10^{-4} ($p = 0.10$) to 5×10^{-5} ($p = 0.20$). This is consistent with the previous values deduced from the thermodynamic experiments (magnetization and specific heat) [27, 32] and the melting line [33]. The *Gi* number and anisotropy parameter as a function of p are shown in figure 4. The anisotropy parameter has a minimum in the vicinity of optimally doped regime, while the *Gi* number is the highest at this regime. The values of *Gi* can also be inferred from the recent detailed study [33] of YBCO at various doping levels (including the vortex lattice melting). They are denoted as red solid triangles in figure 4. Despite the fact that the materials are slightly different (ours is the Ca-doped YBCO, unlike their YBCO), the present values of *Gi* are of the same order of magnitude as those derived in [33]. For small p, from 0.08 to 0.105, the *Gi* value fluctuates in our data but is consistent with that in underdoped YBCO. In the overdoped regime, our results indicate a decreasing *Gi* with p. In the $p = 0.11$–0.14 regime that we did not explore, the data in [33] suggest that the *Gi* has a minimum. This non-monotonic p dependence

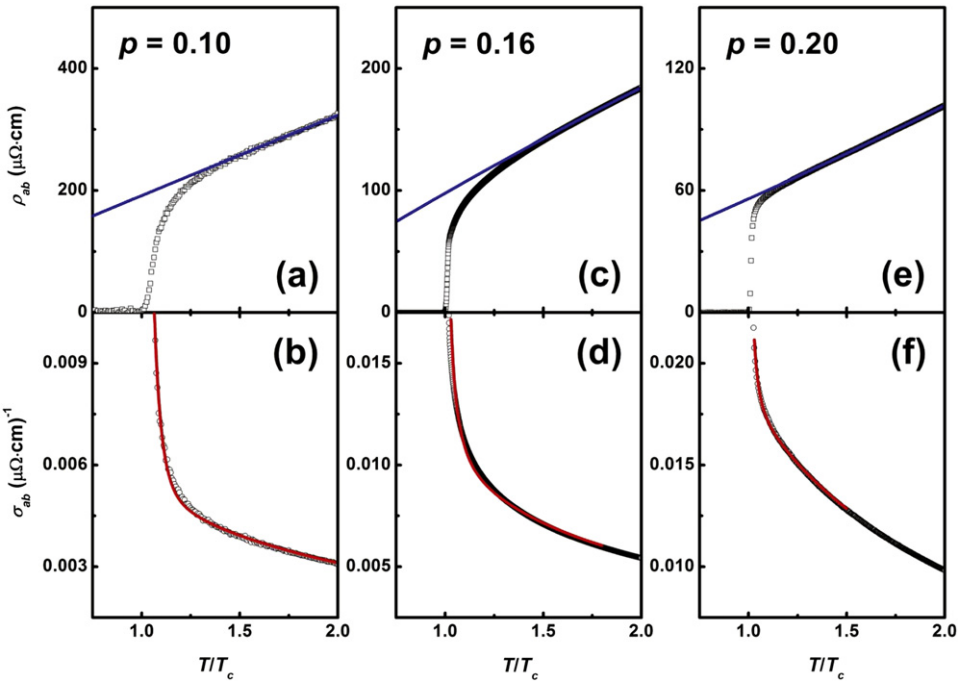

Figure 3. The resistivity and conductivity of the in-plane $Y_{0.7}Ca_{0.3}Ba_2Cu_3O_{7-\delta}$ for (a), (b) $p = 0.10$, (c), (d) $p = 0.16$ and (e), (f) $p = 0.20$ plotted as a function of temperatures normalized at T_c. The blue lines are numerical fits to $\rho(T) = \rho_0 + a_1T + a_2T^2$ with a fitting range as mentioned in section 3.2. The red curves are the theoretical calculations using Ginzburg–Landau description of thermal fluctuations.

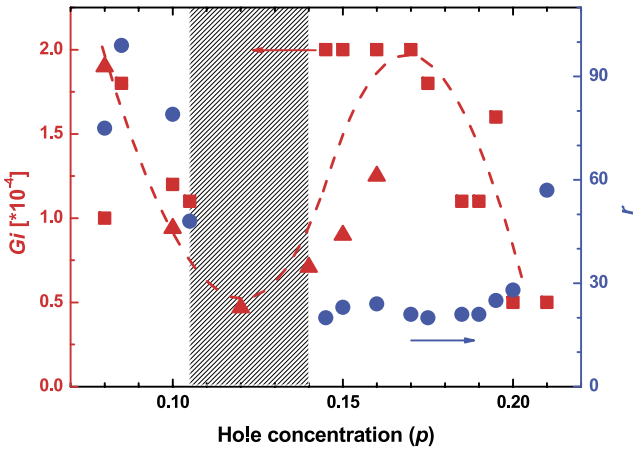

Figure 4. Doping dependences of Ginzburg number *Gi* (red squares: the present work; red triangles: derivations from [33]) and anisotropy parameter *r* (blue circles) in (001)-oriented $Y_{0.7}Ca_{0.3}Ba_2Cu_3O_{7-\delta}$ thin films. The red dashed line is a guide to the eyes. The red triangles represent the values of *Gi* of YBCO derived from [33] for comparison. The gray area is the stripe phase regime.

of *Gi* is similar to that of H_{c2} observed in [4] and [33], and could manifest competing orders in the underdoped regime. With those two parameters, one can estimate T_f as the upper temperature limit of the fluctuation-dominated region. T_f is defined as the temperature region where the effective mass term in LD functional, $\sum_{k=0}^{\Lambda} P_k(0)$, is zero. The momentum cut-off, $\Lambda = 2\pi/\xi_{ab}$, is determined by the coherence length. The thickness of superconducting layer $d = 3.4$ Å was estimated from the neutron experiments [34, 35]. The estimated fluctuation T_f dominated area above T_c is marked with the orange circles in figure 2. In calculations, we assumed that the normal current fluctuations are unaffected by the superconducting fluctuations and we disregard any vortex contribution.

Mean field temperature T_f can be compared with the Nernst temperature from the Nernst signal measurements in YBCO systems [36–41], marked by various open symbols. It is seen that T_f and the Nernst temperature are located in the same temperature range. In general, the Nernst temperature is close to T_f except in the strong stripe phase regime. Therefore, the present comparison suggests a SC fluctuation origin of the Nernst effect. Furthermore, T_f is generally slightly higher than

the Nernst temperature above which the Nernst signal is too small to detect. Consequently, conductance is more sensitive to SC fluctuations than the Nernst voltage is, and serves as a more appropriate tool to study SC fluctuations.

4.2. YBCO phase diagram from RCM

Unlike a sharp resistive transition commonly observed in the conventional superconductors, figure 1 demonstrates the characteristic ρ–T curves in Ca-doped YBCO thin films in a wide doping range. The critical temperature is determined by the middle point transition of $\rho(T)$. The critical temperatures of our samples vary from ∼45 to 85 K. In the vicinity of critical temperature the curvature of $\rho(T)$ varies with the doping. Here we present the analysis of the phase diagram in cuprates following Ando *et al* [17] using the resistivity curvature mapping (RCM) in Ca-doped YBCO.

In figure 2, the curvature ($\mathrm{d}^2\rho^n_{ab}/\mathrm{d}T^2$) of the resistivity curves of Ca-doped YBCO are indicated by colors: the red and blue colors correspond to the positive and the negative curvatures, respectively. The white color represents the curvature close to zero, thereby indicating the linearly temperature-dependent resistivity near the optimally doped regime. The part of phase diagram within the range of $p =$ 0.11–0.14 is not presented due to the stripe phase effect [42] which causes the error in the estimation of p. It is also noted that charge order has been recently proven in YBCO. The charge order has bi-axial structure which is different from the uni-axial stripe order found in the La-based cuprates [43–46]. Using this conductance method alone cannot further explore the extent of the superconducting state and the vicinity of T_c where SC fluctuations cause an abrupt decrease in resistivity. However, the tendency of $T^*(p)$ (light-blue dashed line in figure 2), if extrapolated into the superconducting dome, seems to have a quantum critical point at $p_c \sim 0.21$. This is consistent with the conclusions of Naqib *et al* [11]. Since the extrapolation is qualitative, a higher $p_c \sim 0.24$ due to the recent results by the Nernst effect and resistivity for hole-doped cuprates cannot be excluded [12].

In [17], RCM was only applied to the underdoped and optimally doped regimes. For the present study, RCM was extended from the underdoped to overdoped regimes. Therefore, figure 2 carries more information than the similar plot did in [17]. For example, it was noted in [17] that, departing from being linear in T, $\rho(T)$ is more complicated near room temperature at $p \sim 0.16$. This anomaly was attributed to the complications due to Cu–O chains [17]. The same phenomenon was also observed in the present study near optimal doping. Nevertheless, while the Ca-doped YBCO was optimally doped, it is also highly oxygen deficient. A significant amount of oxygen in Cu–O chains must be removed before the number of doped holes decreases down to optimal doping ($\delta \sim 0.4$ in this case). This is in contrast to the nearly full oxygenation case of YBCO at optimal doping in [17]. Since the similar anomaly in $\rho(T)$ that appeared at $p = 0.16$ was observed for both the fully oxygenated and highly empty Cu–O chains, it is likely associated with the intrinsic dynamics of holes on the CuO_2 planes rather than with the contributions from Cu–O chains.

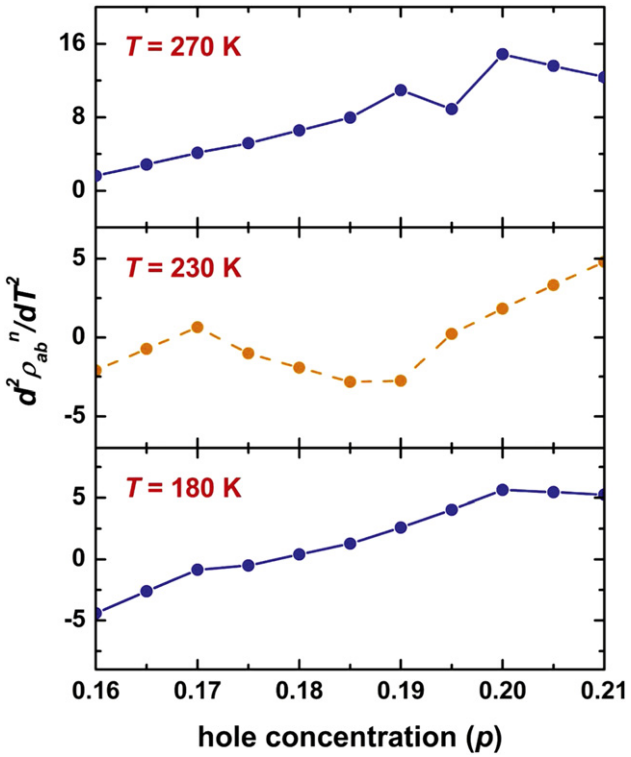

Figure 5. $\mathrm{d}^2\rho^n_{ab}/\mathrm{d}T^2$ for $Y_{0.7}Ca_{0.3}Ba_2Cu_3O_{7-\delta}$ as a function of p within the overdoped region at $T = 180$, 230 and 270 K, respectively. The middle figure emphasizes the sign changes of $\mathrm{d}^2\rho^n_{ab}/\mathrm{d}T^2$ versus hole concentration, different from the behaviors of the other two.

$\rho(T)$ is actually very complicated in the doping regime of $p = 0.15$–0.20. Careful analysis reveals that $\rho(T)$ is not a simple curve with a positive curvature as previously thought. The complications are especially manifested by the isolated blue region in the upper right corner in figure 2. For overdoped samples with $p = 0.18$–0.19, as temperature decreases from room temperature, the curvature of $\rho(T)$ changes sign twice before becoming negative near T_c. Only for heavily overdoped samples with $p > 0.2$ does the curvature of $\rho(T)$ remain always positive above T_c. For further quantitative understanding of $\rho(T)$, we used a model proposed by Hussey *et al* [28–30] to analyze the temperature dependence of $\mathrm{d}^2\rho^n_{ab}/\mathrm{d}T^2$ as a function of p at three temperatures ($T = 180$, 230 and 270 K) in overdoped samples with $p = 0.16$–0.21 (see figure 5). According to the model briefly outlined in section 3.2, the curvature of $\rho(T)$ is expected to increase as p increases. This prediction is consistent with the results of $T = 180$ and 270 K as shown in figures 5(a) and (c). However, at $T = 230$ K, the curvature switches back and forth between positive and negative, as shown in figure 5(b). (This unexpected behavior was also observed in [47], but might have been overlooked then.) Therefore, the complete description of $\rho(T)$ requires a more sophisticated model, albeit that [28–30] might serve as a qualitative approximation.

5. Summary

The comprehensive $\rho(T)$ measurements on Ca-doped YBCO thin films with various hole concentrations from underdoped to overdoped regions (doping levels $p = 0.08$–0.21) reveal fruitful physics. We have calculated the temperature of superconducting fluctuations T_f as a function of hole concentration p using the Ginzburg–Landau model for layered superconductors [16, 21, 22]. Our descriptions of the curvature $d^2\rho_{ab}^n/dT^2$ in the fluctuation-dominated region (above the transition temperature, see the orange curve in figure 2) provide the material parameters like the Ginzburg number and the anisotropy parameter. These results can be considered as evidence that SC fluctuations play a dominant role in this temperature region far above T_c. Comparisons between T_f and the Nernst temperature establish the origin of the Nernst effect as SC fluctuations.

RCM provides a convenient way to analyze the doping-dependent evolution of pseudogap in the whole doping range. The doping dependence of the pseudogap points to the existence of a quantum critical point at $p_c \sim 0.21$–0.24, in agreement with recent results from resistivity and the Nernst signal for Nd-LSCO and YBCO [11, 13–15]. Due to the depleted Cu–O chains near optimal doping for Ca-doped YBCO, the positive curvature of the resistivity appearing at high temperatures likely manifests the intrinsic carrier dynamics of CuO_2 planes, instead of the effects of Cu–O chains. An anomalous sign change of the $\rho(T)$ curvature that appeared near $T \sim 230$ K for $p \sim 0.18$ cannot be accounted for by the argument based on the scattering model [28–30]. More sophisticated theoretical models are needed to fully describe the experimental results from the curvature analysis of $\rho(T)$.

Acknowledgments

The authors are grateful to Dr C H Pan for help in numerical calculations. This work was supported by the National Science Council of Taiwan, ROC under grants: NSC-101-2112-M-009-017-MY2, NSC-101-2112-M-009-020 and NSC-98-2112-M-009-016-MY2 and MOE ATU program at NCTU. Dr P J Lin acknowledges support through UA research index SR-619-1206.

References

[1] Pourret A, Aubin H, Lesueur J, Marrache-Kikuchi C A, Bergé L, Dumoulin L and Behnia K 2006 *Nature Phys.* **2** 683
[2] Klein T, Pribulova Z, Piquerel R, Cercellier H, Marcus J and Marcenat C 2011 *Phys. Rev.* B **83** 094524
[3] Xu Z A, Ong N P, Wang Y, Kakeshita T and Uchida S 2000 *Nature* **406** 486
[4] Chang J *et al* 2012 *Nature Phys.* **8** 751
[5] Grbić M S, Požek M, Paar D, Hinkov V, Raichle M, Haug D, Keimer B, Barišić N and Dulčić A 2011 *Phys. Rev.* B **83** 144508
[6] Li L, Wang Y, Komiya S, Ono S, Ando Y, Gu G D and Ong N P 2010 *Phys. Rev.* B **81** 054510
[7] For a comment on the diamagnetism, see Alexandrov A S 2010 *J. Phys.: Condens. Matter* **22** 426004
[8] Rey R I, Ramos-Álvarez A, Mosqueria J, Ramallo M V and Vidal F 2013 *Phys. Rev.* B **87** 056501
[9] Rullier-Albenque F, Alloul H and Rikken G 2011 *Phys. Rev.* B **84** 014522
[10] Rourke P M C *et al* 2011 *Nature Phys.* **6** 455
[11] Naqib S H, Cooper J R, Tallon J L, Islam R S and Chakalov R A 2005 *Phys. Rev.* B **71** 054502
[12] Hüfner S, Hossain M A, Damascelli A and Sawatzky G A 2008 *Rep. Prog. Phys.* **71** 062501
[13] Daou R *et al* 2009 *Nature Phys.* **5** 31
[14] Daou R *et al* 2010 *Nature* **463** 519
[15] LeBoeuf D *et al* 2010 *Phys. Rev.* B **83** 054506
[16] Larkin A and Varlamov A 2005 *Theory of Fluctuations in Superconductors* (Oxford: Clarendon)
[17] Ando Y, Komiya S, Segawa K, Ono S and Kurita Y 2004 *Phys. Rev. Lett.* **93** 267001
[18] Presland M R, Tallon J L, Buckley B G, Liu R S and Flower N E 1991 *Physica* C **176** 95
[19] Wu K H *et al* 1998 *Japan. J. Appl. Phys.* **37** 4346
[20] Ando Y, Segawa K, Lavrov A N and Komiya S 2003 *J. Low Temp. Phys.* **131** 793
[21] Rosenstein B and Li D 2010 *Rev. Mod. Phys.* **82** 109
[22] Tinkham M 1996 *Introduction to Superconductivity* (New York: Dover)
[23] Kovner A and Rosenstein B 1989 *Phys. Rev.* D **39** 2332
[24] Kleinert H 1995 *Path Integrals in Quantum Mechanics, Statistics, and Polymer Physics* (Singapore: World Scientific)
[25] Cabo L, Mosqueira J and Vidal F 2007 *Phys. Rev. Lett.* **98** 119701
[26] Ong N P, Wang Y, Li L and Naughton M J 2007 *Phys. Rev. Lett.* **98** 119702
[27] Li D and Rosenstein B 2003 *Phys. Rev. Lett.* **90** 167004
[28] Abdel-Jawad M, Analytis J G, Balicas L, Carrington A, Charmant J P H, French M M J and Hussey N E 2007 *Phys. Rev. Lett.* **99** 107002
[29] Hussey N E, Abdel-Jawad M, Carrington A, Mackenzie A P and Balicas L 2003 *Nature* **425** 814
[30] Abdel-Jawad M, Kennett M P, Balicas L, Carrington A, Mackenzie A P, Mckenzie R H and Hussey N E 2006 *Nature Phys.* **2** 821
[31] Presland M R, Tallon J L, Buckley R G, Liu R S and Flower N E 1991 *Physica* C **176** 95
[32] Li D and Rosenstein B 2004 *Phys. Rev.* B **70** 144521
[33] Ramshaw B J, Day J, Vignolle B, LeBoeuf D, Dosanjh P, Proust C, Taillefer L, Liang R, Hardy W N and Bonn D A 2012 *Phys. Rev.* B **86** 174501
[34] Jorgensen J D, Veal B W, Paulikas A P, Nowicki L J, Crabtree G W, Claus H and Kwok W K 1990 *Phys. Rev.* B **41** 1863
[35] Palles D, Liarokapis E, Leventouri T and Chakoumakos B C 1998 *J. Phys.: Condens. Matter* **10** 2515
[36] Wang Y, Li L and Ong N P 2006 *Phys. Rev.* B **73** 024510
[37] Rullier-Albenque F, Tourbot R, Alloul H, Lejay P, Colson D and Forget A 2006 *Phys. Rev. Lett.* **96** 067002
[38] Wang Y, Ong N P, Xu Z A, Kakeshita T, Uchida S, Bonn D A, Liang R and Hardy W N 2002 *Phys. Rev. Lett.* **88** 257003
[39] Li P, Mandal S, Budhani R C and Greene R L 2007 *Phys. Rev.* B **75** 184509
[40] Chang J *et al* 2010 *Phys. Rev. Lett.* **104** 057005
[41] Kokanović I, Cooper J R and Matusiak M 2009 *Phys. Rev. Lett.* **102** 187002
[42] Liang R, Bonn D A and Hardy W N 2006 *Phys. Rev.* B **73** 180505
[43] Wu T, Mayaffre H, Krämer S, Horvatić M, Berthier C, Hardy W N, Liang R, Bonn D A and Julien M-H 2011 *Nature* **477** 191
[44] Laliberté F *et al* 2011 *Nature Commun.* **2** 432
[45] Ghiringhelli G *et al* 2012 *Science* **337** 821
[46] Chang J *et al* 2012 *Nature Phys.* **8** 871
[47] Tallon J L, Loram J W and Panagopoulos C 2003 *J. Low Temp. Phys.* **131** 387